Progress In Electromagnetics Research, Vol. 143, 105–130, 2013

A SYSTEMATIC DESIGN PROCEDURE FOR MICROSTRIP-BASED UNIDIRECTIONAL UWB ANTENNAS

Purna B. Samal[1, 2], Ping Jack Soh[1, 3, *], and Guy A. E. Vandenbosch[1]

[1]ESAT-TELEMIC, Katholieke Universiteit Leuven, Kasteelpark Arenberg 10, Leuven 3001, Belgium

[2]Electronics and Communication Department, College of Science and Technology, Rinchending, Phuentsholing, Bhutan

[3]School of Computer and Communication Engineering, Universiti Malaysia Perlis (UniMAP), Pauh Putra Campus, Arau, Perlis 02600, Malaysia

Abstract—A design procedure for microstrip antenna topologies operating within the full UWB band is described. The presence of the full ground plane successfully results in a unidirectional antenna, which is important in applications related to Wireless Body Area Networks (WBAN). The existing broadbanding concepts have been creatively combined throughout the design to enable the UWB behavior, while simultaneously keeping the full ground plane intact. The procedure is validated with a concrete design of a microstrip type UWB antenna operating from 3.6 GHz to 10.3 GHz.

1. INTRODUCTION

In the last few decades the microstrip antenna topology has been extensively investigated due to its attractive features such as low profile, low cost, and fabrication simplicity. Due to these features, microstrip antennas are popularly used in many wireless communication applications. However, one of the major drawback of the microstrip topology is its narrow bandwidth. Upon the introduction of Ultra Wideband (UWB) technology in 2002, extensive research efforts were channeled towards realizing planar antennas operating between 3.1 and 10.6 GHz [1]. High data rate

Received 16 September 2013, Accepted 21 October 2013, Scheduled 28 October 2013

* Corresponding author: Ping Jack Soh (pingjack.soh@esat.kuleuven.be).

transmission capabilities with low power spectral densities [1–3] are the attractive features of UWB over conventional (narrow band) wireless communication techniques [4].

More recently, the application of UWB has been extended into the area of Wireless Body Area Networks (WBAN) thanks to its potential in enabling worn communications [5]. In such setting, planar textile-based antennas are extremely suitable to ensure flexibility, conformality and ergonomocity [6–9]. Moreover, the properties of the designed antenna and the avoidance of on-body detuning are critical in further facilitating a reliable communication link. Recently, proposed designs for wideband BAN are based on monopole and Vivaldi topologies, fed either using a microstrip or a coplanar waveguide (CPW) transmission line [10–16]. Their wide bandwidth behavior is typically enabled by cutting slots in the ground plane, or by implementing partial rear ground planes. Such topologies are disadvantageous as they radiate at both the forward and backward directions. Such property inherently introduces a strongly coupling to the human body when worn.

In this work, a systematic procedure is described to design antennas with a full rear ground plane, mitigating the body detuning. Besides detailing the broadbanding principles involved, the design procedure to combine all these concepts is presented in detail. It will be shown that reaching UWB features using the inherently narrowband microstrip topology is possible. The procedure can be used to produce different antennas with different shapes suited for different situations.

2. TEXTILE AND MATERIALS

Although the main topic in this paper is the design procedure itself, this procedure cannot be efficiently explained and illustrated without having a concrete antenna in mind. A full-textile antenna is chosen as target. It has to be emphasized however that the topology obtained is by no means the only solution. Many more concrete topologies, based on the same design principles can be conceived, depending on the choices made by the designer. Two textiles are used: Shieldit Super as the conductor (for radiators and ground plane) and felt as the dielectric (for the substrate). ShieldIt Super from LessEMF Inc. is a 0.17 mm thick, flexible conductive textile. Its conductivity is estimated using the procedure proposed in [17], resulting in a value of 1.18×10^5 S/m. Felt is a 3 mm thick, thermally-isolating textile with a relative permittivity ε_r of 1.45 and a loss tangent $\tan\delta$ of 0.044. A 50 Ω SMA connector model 546-3181 from RS Components is used to feed the antenna from its reverse side. Simple manual cutting tools

were used to fabricate the designed antenna as specified in [17].

3. DESIGN PROCEDURE

As in conventional antenna design procedures, the design process is initiated with a theoretical calculation to estimate the antenna dimensions. In our case, these initial dimensions are calculated based on the well-known procedure explained in [18] to estimate the size of two rectangular microstrip antennas, one at 5 GHz and another at 7 GHz. Next, various broadbanding techniques are added in a sequential manner, with the specific aim of maintaining the full ground plane. The effect of each broadbanding technique is studied by evaluating the antenna's basic performance parameters, i.e., the reflection coefficient (S_{11}), realized gain, radiation pattern and radiation efficiency, using CST Microwave Studio [19]. The initial CST simulations are performed using the transient solver with low-mesh settings prior to detailed, high-mesh simulations. This low-mesh-high-mesh strategy is computationally very efficient and proved to be an essential part of the design procedure, as critical and non-critical antenna parameters are easily distinguishable from the results. Each implemented technique and its respective bandwidth improvement will be systematically discussed. As more techniques are incorporated into the structure to achieve the UWB behavior, the antenna experiences a gradual increase in complexity.

Figures 1(a)–(b) show the CST-optimized dimensions of two rectangular microstrip antennas resonating at 5 and 7 GHz, respectively, with their simulated reflection coefficients (S_{11}) shown in Fig. 1(c). As expected for a microstrip structure, the obtained bandwidth is relatively narrow, i.e., 462 MHz for the 5 GHz patch and 589 MHz for the 7 GHz patch.

Once the basic microstrip structures have been optimized, various broadbanding techniques [20] are then applied for bandwidth enhancement. The various techniques, which are sequentially implemented, are listed as follows:

3.1 resonance overlapping,

3.2 slot,

3.3 parasitic patch,

3.4 Vivaldi blending,

3.5 stepped notch,

3.6 rectangular and T-shape slits.

Each technique's contribution towards the resulting bandwidth and its effect on the structure's gain, radiation efficiency and radiation

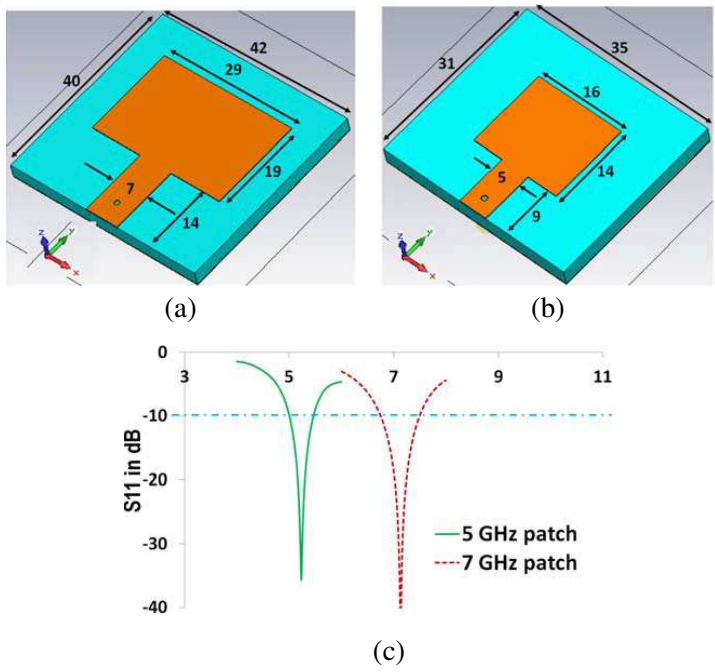

Figure 1. Optimized dimensions of the microstrip antennas designed at (a) 5 GHz, (b) 7 GHz and (c) simulated S_{11}.

patterns are also presented consecutively, as the antenna evolves towards achieving a UWB behavior.

3.1. Resonance Overlapping (RO)

An effective broadbanding method is to combine two closely-spaced resonances. This is implemented by connecting both radiating structures via a single feed line as shown in Fig. 2(a) [21–23]. The upper patch operates in the lower 5 GHz frequency band whereas the smaller patch at the bottom in the higher 7 GHz frequency band. This technique effectively enlarges the overall bandwidth to 3.89 GHz. Next, impedance matching of the feed line is further improved by introducing a single step transition, prior to further optimization. This results in an additional bandwidth of 280 MHz (i.e., a total bandwidth of 4.17 GHz). Resulting dimensions and S_{11} are shown in Figs. 2(b) and 2(c), respectively. The comparison of gains for this feed line modification depicted in Fig. 2(c) also indicates no significant degradation.

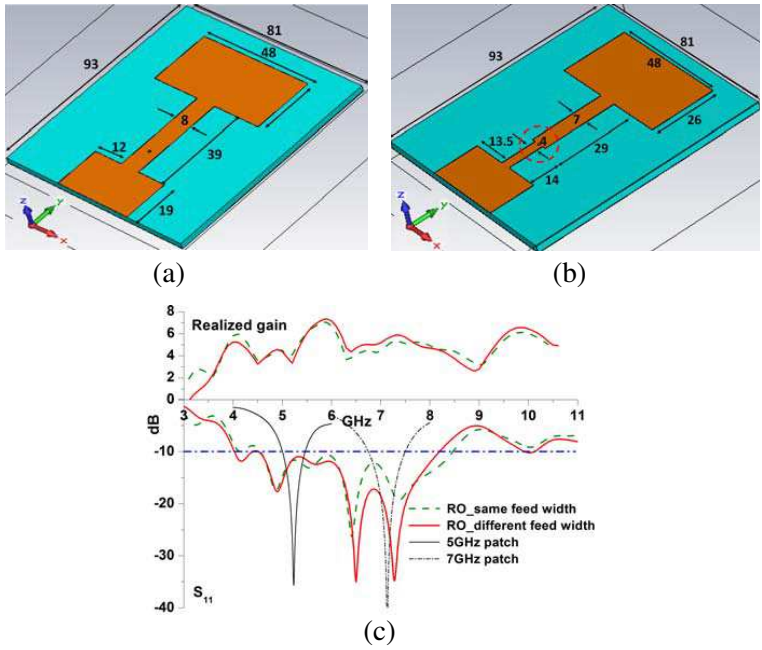

Figure 2. Combined structure for resonance overlapping (RO) with (a) conventional feed (same feed width), (b) modified feed (different feed width) and (c) comparison of their S_{11} and realized gain.

The major drawback of implementing solely this technique is an increased overall antenna size. Typical microstrip antennas resonating at 5 GHz and 7 GHz feature overall areas of 1680 mm^2 (42×40 mm^2) and 1085 mm^2 (32×35 mm^2), respectively. Thus the antenna size is enlarged to 7533 mm^2, i.e., 93×81 mm^2, corresponding to a 7 time increment.

3.2. Slot

The slotting method implemented in this section is capable of reducing the overall antenna size besides providing a dual resonant mode [24]. A circular slot is incorporated into the smaller (bottom) radiator of the previous structure prior to re-optimization. As shown in Fig. 3(a), the total area of the new antenna is now reduced to 6612 mm^2 (87×76 mm^2), translating into a 1.14 reduction factor. The dual resonance achieved by the circular slot is visible in Fig. 3(c), resulting in a total bandwidth of 4.6 GHz from two separate bands: 1.2 GHz (from 4.3 to 5.5 GHz) and 3.4 GHz (from 6.7 to 10.1 GHz), with a band notch

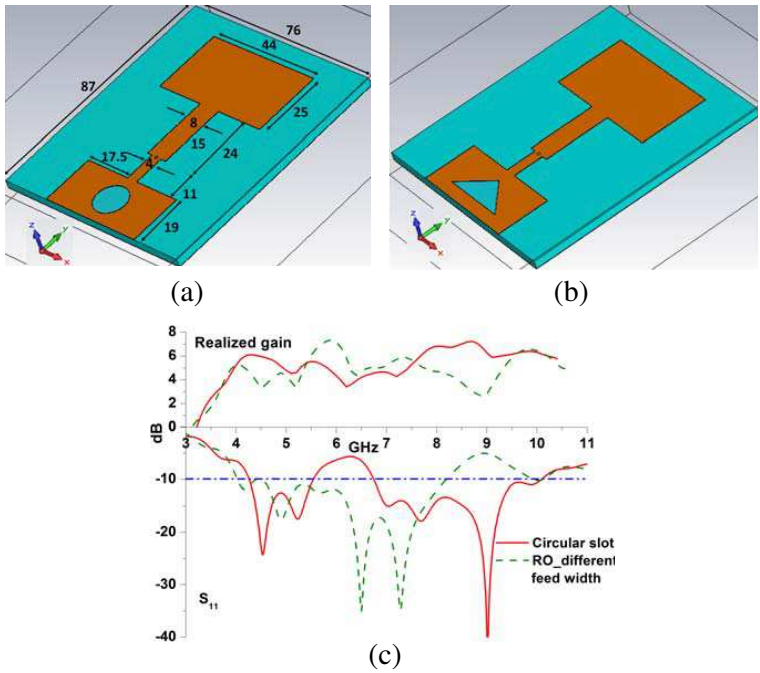

Figure 3. Two similarly-dimensioned antennas with (a) circular slot, and (b) triangular slot. (c) S_{11} and realized gain for structure in (a).

at c.a. 6 GHz. In comparison to the previous structure, an additional 430 MHz bandwidth is achieved. Also, the realized gain has improved.

The radiation patterns of the previous and the current structure in xz and yz plane at 5 GHz and 7 GHz are shown in Fig. 4. In general, a symmetrical pattern is observed in the xz plane due to symmetry, whereas in the yz plane, an omnidirectional pattern with sharp nulls is seen. In the xz plane at 5 GHz, the circular slot eliminates the sharp nulls at $\varphi = 30°$ and $-30°$, providing a smooth, broad forward beam. In the yz plane, the main lobe is shifted to precisely $\varphi = 0°$ when the slot is present. A 4 dB increment in the main lobe magnitude is observed compared to a 1 dB improvement provided by the previous structure, as seen in Table 1. No significant pattern changes are observed in the yz plane at 7 GHz. The xz plane angular width is decreased by 53.5°. A detailed comparison is presented in Table 1.

Other slot shapes were also investigated, i.e., triangular and rectangular, see Fig. 3(b). The total slot area was maintained at 131 mm^2 to provide a valid comparison, while keeping all other antenna dimensions fixed. The S_{11} are presented in Fig. 5. It is observed

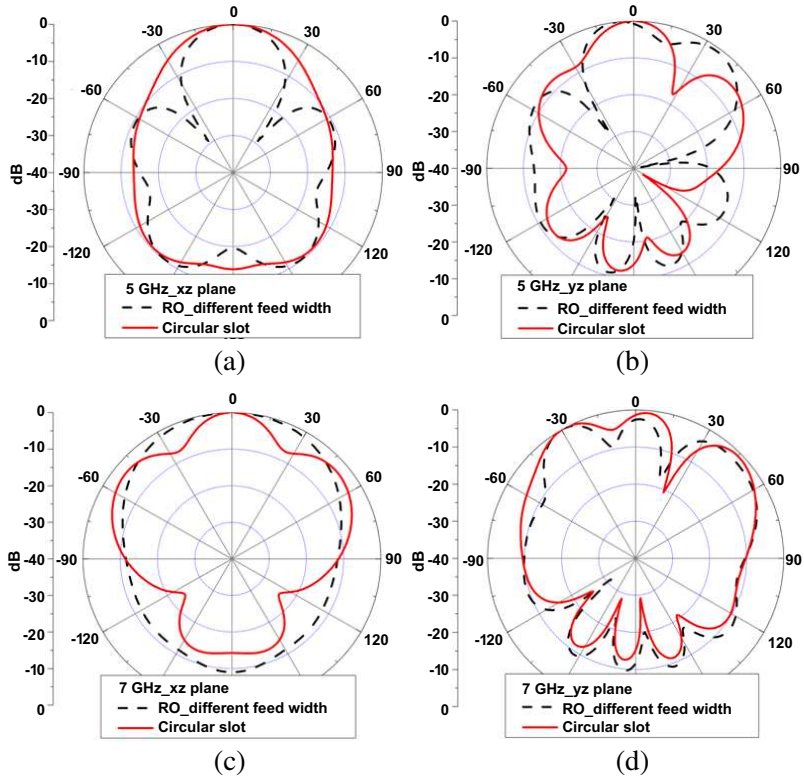

Figure 4. Simulated radiation pattern comparison for (a) xz plane at 5 GHz, (b) yz plane at 5 GHz, (c) xz plane at 7 GHz, and (d) yz plane at 7 GHz.

that the circular and rectangular slots behave similarly, whereas the triangular slot reduces the bandwidth by 650 MHz.

3.3. Parasitic Patch

Since the lowest operating frequency of the resulting structure is ca. 4.3 GHz, the next objective is to increase the bandwidth in the lower operating band. This can be achieved by introducing a parasitic patch, which is expected to also facilitate lowering the overall resonance band [25] through the capacitive coupling effect [20]. A parasitic patch is added and optimized, as shown in Fig. 6. The large-size parasitic patch more than doubles the lower frequency bandwidth (from 1.2 GHz to 2.6 GHz), by lowering the lowest operating frequency from 4.3 GHz to 3.5 GHz. The optimized antenna operates from 3.5 to 6.1 GHz.

Table 1. Comparison of radiation pattern properties.

Freq. (GHz)	Plane	Details	RO with different feed width	Circular slot	Parasitic patch	Vivaldi effect	Stepped notch
5	*xz*	Realized Gain (dB)	0.3	5.0	4.8	NA	Please refer to Table 2
		Main lobe direction (°)	0.0	0.0	0.0		
		3 dB angular width (°)	32.9	45.4	38.4		
		Side lobe level (dB)	−10.2	−10.5	−15.6		
	yz	Realized Gain (dB)	1.0	5.0	4.8		
		Main lobe direction (°)	−6.0	0.0	0.0		
		3 dB angular width (°)	26.0	27.8	23.7		
		Side lobe level (dB)	−1.0	−5.2	−6.5		
7	*xz*	Realized Gain (dB)	0.2	1.8	1.2	0.3	1.2
		Main lobe direction (°)	0.0	0.0	0.0	0.0	0.0
		3 dB angular width (°)	81.8	28.3	25.4	22.4	24.2
		Side lobe level (dB)	−9.0	−3.1	-8.0	−4.2	−6.7
	yz	Realized Gain (dB)	2.8	2.3	2.0	0.5	2.9
		Main lobe direction (°)	−30.0	5.0	−5.0	−34.0	−33.0
		3 dB angular width (°)	21.7	23.4	18.4	19.7	21.0
		Side lobe level (dB)	−2.4	−1.7	−2.2	−2.0	−1.7

Legend: NA = not evaluated due to poor performance at this frequency (S_{11} > -10 dB).

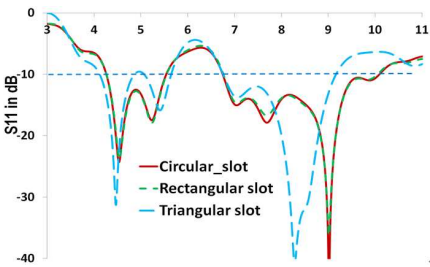

Figure 5. Comparison of S_{11} for 3 slot shapes.

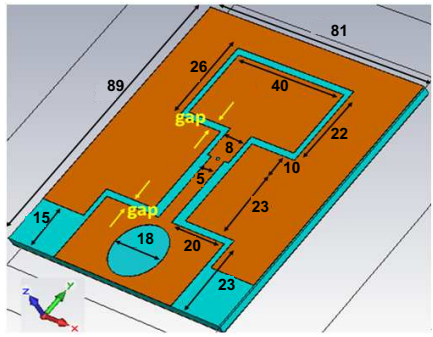

Figure 6. Optimized structure dimensions with the parasitic patch.

Simultaneously, a gain improvement of ca. 3 dB is achieved at 3.5 GHz, see Fig. 7(a). A similar improvement can also be seen between 5.5 and 6 GHz. On the contrary, a 2 dB average reduction in realized gain is observed due to the impedance matching degradation between 7

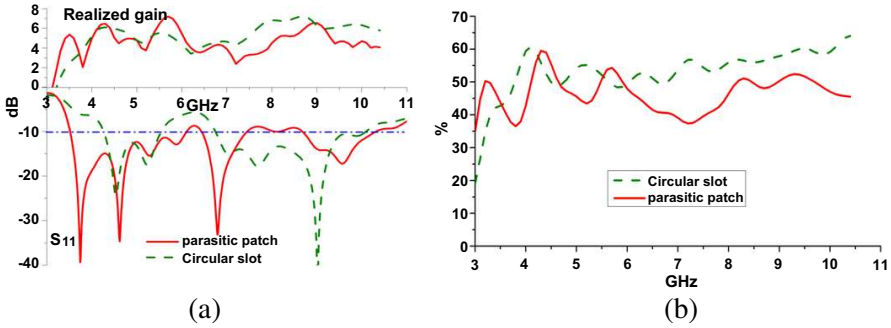

Figure 7. Comparison of (a) simulated S_{11} and realized gain, and (b) radiation efficiency.

and 9 GHz. Moreover, the additional parasitic patch also decreases the radiation efficiency by 10.3% (average) above 6 GHz, as shown in Fig. 7(b). The new structure's radiation patterns are also analyzed in comparison with the previous structure at 5 and 7 GHz and shown in Fig. 8. With the addition of the parasitic patch a more directive radiation pattern is visible at 5 GHz in xz plane, whereas a more omni-directional radiation is observed at 7 GHz. In general, a small reduction in angular width (around 5°) is noticed, making the xz patterns at both frequencies more directional with simultaneous side lobe reductions, see Table 1.

Next, the effect of the capacitive coupling is studied. It is well-known that the magnitude of the capacitive coupling directly depends on the size of the gap between the main patch and the parasitic patch. A higher capacitive coupling occurs for a smaller gap. This can be used to further enlarge the bandwidth. As is clearly visible in Fig. 9, a gap of 1 mm results in the highest bandwidth. However, since fabrication is done manually, a minimum gap of 2 mm is chosen in order to reduce the relative fabrication error around the two rectangular patches. This area is labeled in Fig. 6, representing the smallest distance between the two patches and the parasitic patch. The parasitic patch's dimension was increased/decreased so that it may be edged closer to/further away from the two rectangular patches to achieve the required gap size, as the dimensions of the latter were kept constant.

3.4. Vivaldi Blending

The previous two methods have effectively lowered and enlarged the lower operating band. However, the impedance matching at higher frequencies becomes poorer, see Fig. 7(a). This is related to the well-

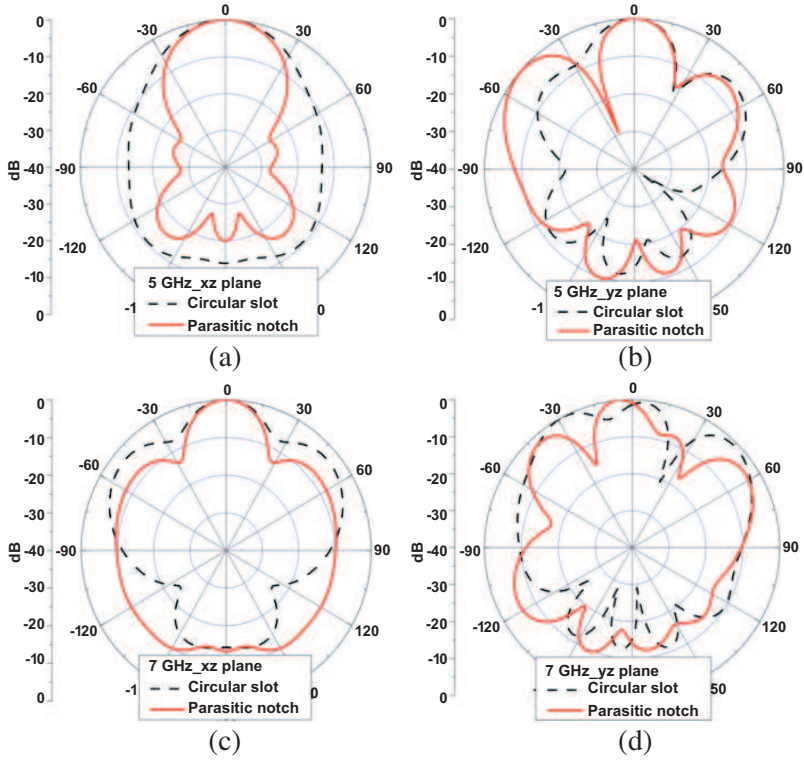

Figure 8. Comparison of simulated radiation patterns for (a) xz plane at 5 GHz, (b) yz plane at 5 GHz, (c) xz plane at 7 GHz, and (d) yz plane at 7 GHz.

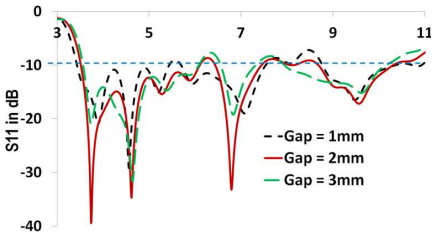

Figure 9. The effect of gap size between the main and parasitic radiators.

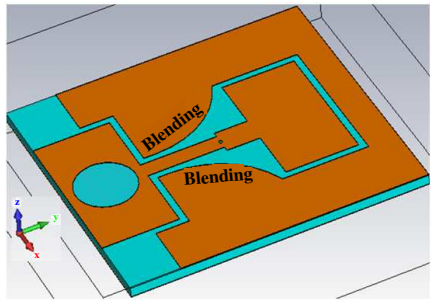

Figure 10. Blending the parasitic patch.

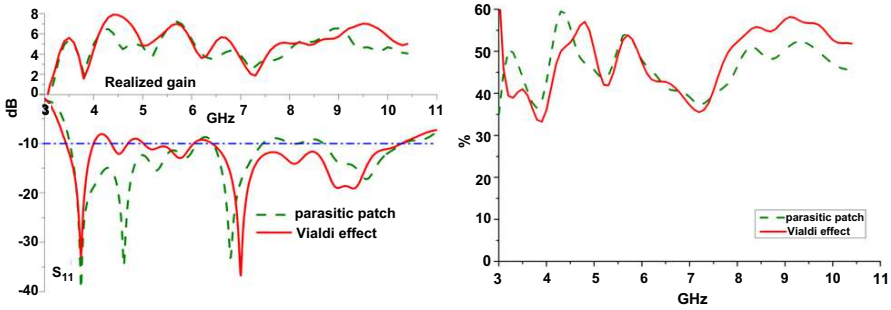

(a) (b)

Figure 11. Comparison of (a) simulated S_{11} and realized gain, and (b) radiation efficiency.

known fact that in many cases there is a tradeoff between impedance matching quality and bandwidth, especially for UWB antennas. The Vivaldi concept can be used to overcome this, as it is able to intrinsically provide a real broadband impedance matching [13, 14]. Moreover, it can be used in such a way that it only affects the impedance tuning in the higher frequency band, maintaining the existing lower frequency bandwidth. The Vivaldi concept is realized by blending the parasitic edges with a radius of 27 mm, as shown in Fig. 10, with all other dimensions kept constant (as the dimensions shown in Fig. 6). After proper optimization, an improved impedance matching in the higher frequency band with acceptable bandwidth degradation at the lower frequencies is obtained, see Fig. 11(a), yielding a 6.8 GHz bandwidth. Realized gain and radiation efficiency are also compared with the ones of the previous structure in Fig. 11. An average radiation efficiency improvement of 6% is observed above 7.5 GHz. The radiation patterns at 7 GHz in both xz and yz plane are not significantly changed, as shown in Fig. 12. An increase of the side lobe magnitude by 4 dB is observed in the xz plane, whereas blending improves slightly the omni-directional characteristic in the yz planes. Further details are tabulated in Table 1.

3.5. Stepped Notch

The blending method successfully improves the antenna matching above 7 GHz. However, besides degradation below this frequency, the operation at the UWB highest frequency of 10.6 GHz has also not been achieved, see Fig. 11(a). Stepped notches can be used to overcome this. It was reported in [26] that the use of a stepped notch between the radiating patch and its feed line is capable of tuning a structure's capacitance, possibly improving impedance matching

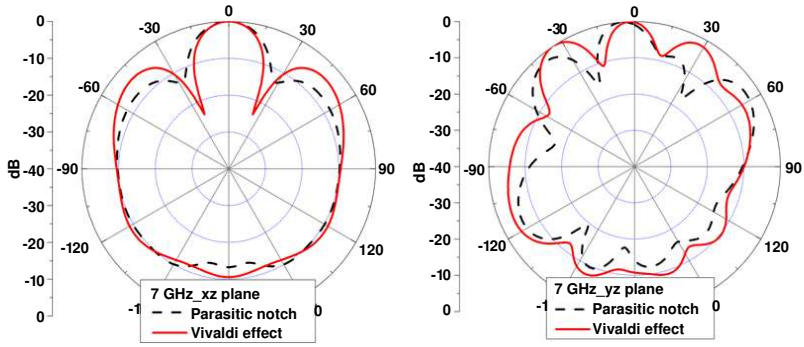

Figure 12. Comparison of simulated radiation patterns at 7 GHz.

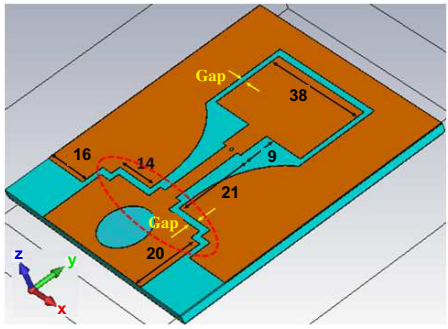

Figure 13. Optimized structure dimensions with stepped notches.

towards a broader bandwidth. In this antenna, the stepped notches are placed between the feed line and the lower radiator, which initially operated at 5 GHz, see circled area in Fig. 13. Capacitance tuning is also used to extend the upper limit of the existing bandwidth. The optimized dimensions obtained in the previous section were used as the initial dimensions for further optimization with notches. The optimal dimensions of the first and second stepped notch located nearest to the feed line are $2 \times 4\,\text{mm}^2$ and $14 \times 3\,\text{mm}^2$, respectively. The $89 \times 81\,\text{mm}^2$ overall antenna size and the 2 mm capacitive gap between the main and parasitic patch remain the same. The main patch's dimensions were re-optimized to accommodate the impedance changes caused by the two stepped notches. This method successfully improves impedance matching between 4.4 GHz and 6 GHz, besides broadening the bandwidth by ca. 560 MHz compared to the previous topology. This also extends the upper bandwidth limit to ca. 10.5 GHz without compromising the existing matching and bandwidth above 7 GHz, as

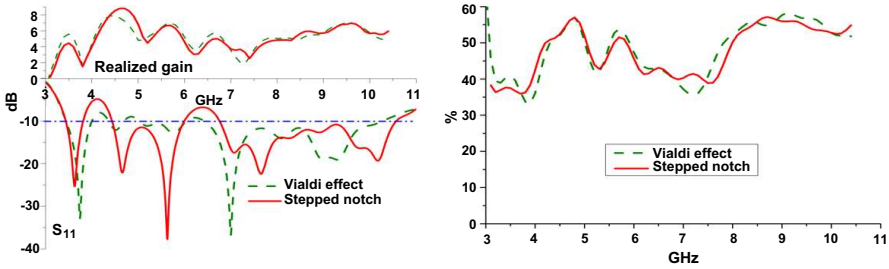

(a) (b)

Figure 14. Comparison of (a) simulated S_{11} and realized gain, and (b) radiation efficiency.

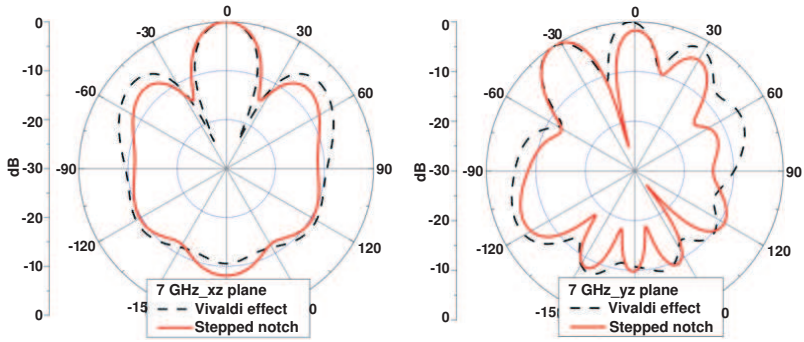

Figure 15. Comparison of simulated radiation patterns at 7 GHz.

shown in Fig. 14(a). However, this structure also comes with a cost — the existence of a larger band notch from 3.8 to 4.4 GHz, and from 6 to 7 GHz. This can be resolved using a combined stepped notch-blending technique, which will be explained in the following sections. A consistent realized gain, with less than 0.5 dB variation is shown between 8 and 10.4 GHz for this notch-integrated structure. However, between 4.5 and 5 GHz, a larger 1 dB variation is seen, with a peak realized gain of 8.8 dB at 4.7 GHz. Radiation efficiency also behaves similarly for the two topologies as shown in Fig. 14(b). The effect of the stepped notches on the radiation pattern at 7 GHz can be seen in Fig. 15. A detailed comparison is presented in Table 1.

3.6. T-shaped Slits

The use of the two stepped notches in the previous section easily improves impedance matching between 4.4 and 6 GHz with further bandwidth increment below 7 GHz. However, as explained earlier, it

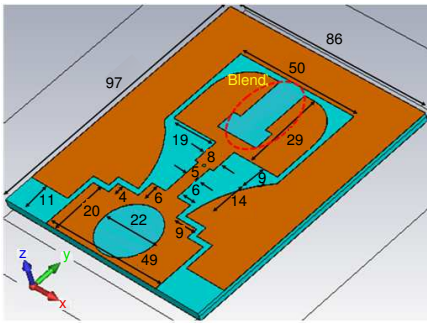

Figure 16. Optimized structure dimension with T-shaped slit.

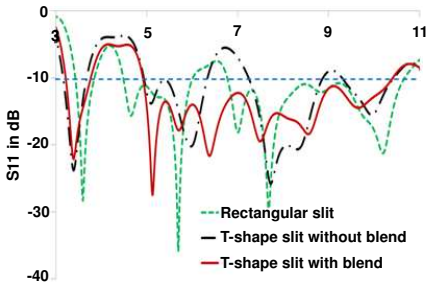

Figure 17. S_{11} comparison with different slits and blends.

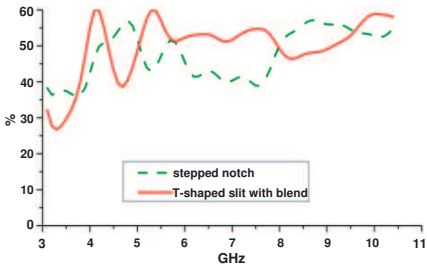

Figure 18. Comparison of the radiation efficiency.

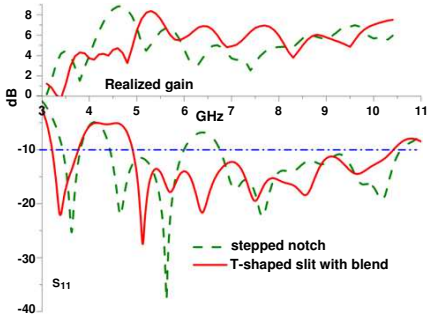

Figure 19. Comparison of S_{11} and realized gain.

worsens the characteristics around 4 GHz and between 6 and 7 GHz. The next aim is to first eliminate the band notch between 6 and 7 GHz. This is done by introducing a slit in the upper radiator [27]. Initially a single rectangular slit was introduced. This was then improved to a T-shaped slit, as shown in Fig. 16 and indicated by a dotted circle. The optimized dimensions of this slit are $11 \times 17\,\text{mm}^2$ and $7 \times 17\ \text{mm}^2$. The resulting S_{11} for this structure is shown in Fig. 17. However, further impedance matching degradation was observed between 3.6 and 4.9 GHz and between 6.7 and 7 GHz. As in Section 3.4, this is mitigated by tuning the capacitive coupling between top radiator and the parasitic patch through the incorporation of edge blends in the top radiator. An optimal blend radius of 13 mm was found. The S_{11} response of this blended structure with the T-shaped slit is also shown in Fig. 17, indicating the effective removal of the band notch from 6 to 7 GHz. The S_{11} and realized gain of the resulting T-slit blended

radiator is compared to the ones of the stepped notch structure in Fig. 19, indicating a 5.6 GHz bandwidth from 4.9 to 10.5 GHz. An additional 560 MHz of bandwidth is also achieved between 3 and 4 GHz, separated from the higher operating band by a 1 GHz-wide band notch located between 4 and 5 GHz. A realized gain variation between 4 dB at 8.3 GHz and 8.5 dB at 5.3 GHz is observed above 5 GHz. The addition of the T-shaped slit has reduced the gain significantly between 4 and 5 GHz. Meanwhile, the radiation efficiency shown in Fig. 18 has increased by more than 10% between 6 and 8 GHz compared to the previous structure. The radiation patterns at 5.5 GHz and 8 GHz are shown in Fig. 20. A decrease in the 3-dB angular width in the xz plane at both frequencies and a reduction of the far side lobe level in the yz plane are observed. The xz plane experiences an increase in side lobe levels by several dB. However, in this plane the main lobe is now directed towards 0° via the use of this technique. This is all detailed in Table 2.

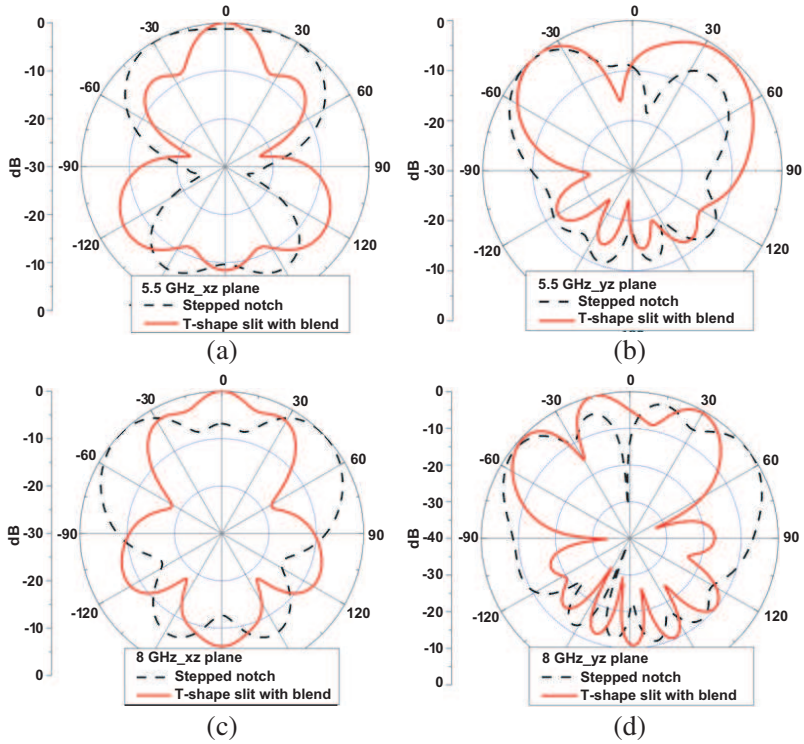

Figure 20. Comparison of simulated radiation patterns for (a) xz plane at 5.5 GHz, (b) yz plane at 5.5 GHz, (c) xz plane at 8 GHz, and (d) yz plane at 8 GHz.

Table 2. Comparison of radiation patterns of stepped notch topology and T-shape slit blend topology.

Freq. (GHz)	Plane	Details	Stepped notch	T-shape slit with blend
5.5	xz	Realized Gain (dB)	−7.9	−9.7
		Main lobe direction (°)	28.0	0.0
		3 dB angular width (°)	100.0	26.3
		Side lobe level (dB)	−5.5	−5.4
	yz	Realized Gain (dB)	0.1	−1.2
		Main lobe direction (°)	−44.0	−40.0
		3 dB angular width (°)	38.6	33.7
		Side lobe level (dB)	−5.4	−11.9
8.0	xz	Realized Gain (dB)	−2.9	−1.6
		Main lobe direction (°)	46.0	0.0
		3 dB angular width (°)	44.3	29.1
		Side lobe level (dB)	−5.9	−2.5
	yz	Realized Gain (dB)	24.2	3.4
		Main lobe direction (°)	54.0	−14.0
		3 dB angular width (°)	35.5	17.7
		Side lobe level (dB)	−2.5	−10.2

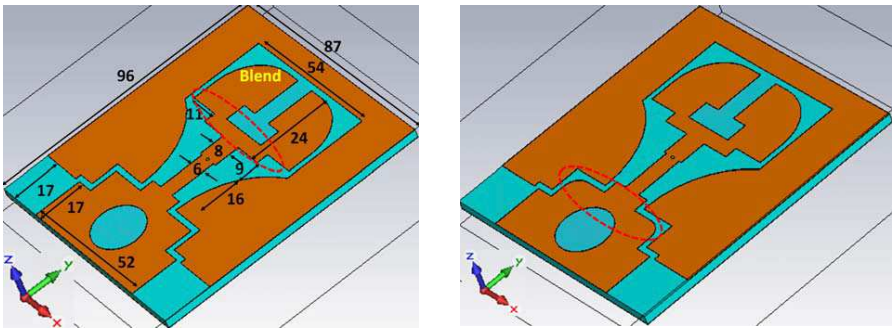

Figure 21. Optimized structure dimensions with (a) single step notch, and (b) notch with blending.

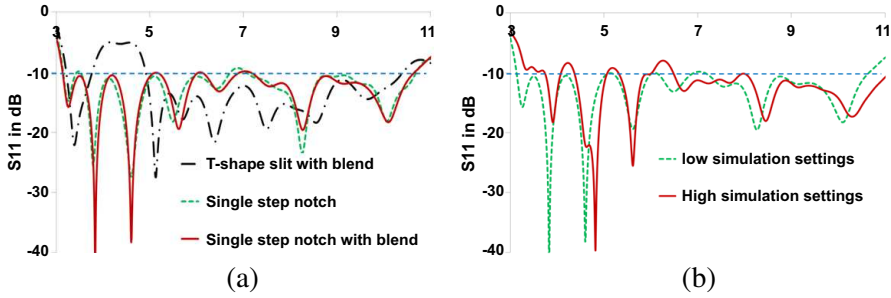

Figure 22. (a) S_{11} for previous (T-shape) and two new stepped notch topologies, and (b) S_{11} of resulting structure using different simulation settings.

3.7. Final Topology

In this section the remaining band notch between 4 and 5 GHz (see Fig. 19) is removed with the step notch method and the blending method, two techniques already used before. A single step notch is introduced between the feed line and the top radiator. The optimized dimensions of this step notch are $10 \times 4\,\text{mm}^2$, as shown in Fig. 21(a), marked by a red dotted circle and listed in Table 3. The resulting S_{11} is shown in Fig. 22(a). To achieve a better impedance matching, blending is introduced in the second step notch of the circularly-slotted lower radiator, as circled in Fig. 21(b). The optimal blending radius is found to be 5 mm. All other antenna dimensions are kept constant. The resulting bandwidth spans 7.5 GHz, i.e., the full UWB band from 3.1 to 10.6 GHz, see Fig. 22(a).

Table 3. Optimized dimensions of the final ATA-FGP.

Modification	Dim. (mm)	Remarks
T-shaped slit	7×17 18×8	On the top radiator
Two stepped notches	(1) 4×5 (2) 13×10	Transition from feed line to the bottom radiator
Circular slot radius	9	On the bottom radiator
Blending radius	16	On the top radiator

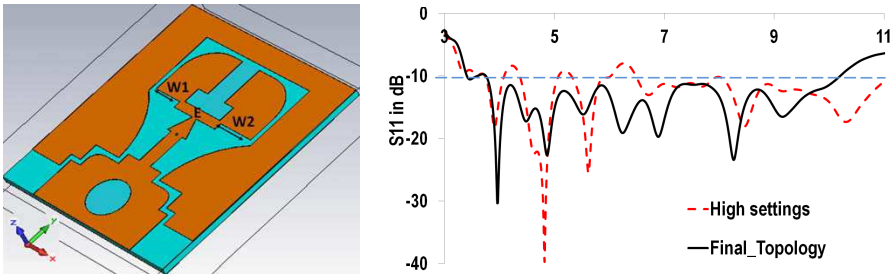

(a) (b)

Figure 23. (a) Final topology of the ATA-FGP and (b) comparison of the optimized S_{11} between the initial and different mesh settings.

Table 4. Summary of all used techniques, purposes and their resulting effects in achieving UWB behavior.

Techniques used	Purpose	Bandwidth (*BW*)	Effect
Resonance overlapping	To broaden bandwidth by combining two closely-spaced resonances.	Improved *BW* by 2.84 GHz	Enlarged the overall bandwidth to 3.89 GHz, but also increased the overall antenna size by a factor of 7.
Circular slot	To reduce overall antenna size while maintaining the dual band behavior.	Improved *BW* by 430 MHz.	Reduced the overall antenna size by a factor of 1.14.
Parasitic patch	To increase bandwidth in the lower operating band through capacitive coupling.	Improved *BW* in the lower frequency band by 800 MHz.	Lowered the operating frequency range from 4.3 to 3.5 GHz, but reduced impedance matching at the higher frequencies.
Vivaldi blending	To provide better impedance tuning in the higher frequency band by blending the parasitic edges.	Improved *BW* by 3.5 GHz above 6.5 GHz.	Improved impedance matching at the higher frequencies with a slight impedance matching degradation below 6.5 GHz.
Stepped Notch	To improve impedance matching at lower frequencies through capacitive tuning without degrading existing bandwidth above 7 GHz.	Broadened *BW* by 560 MHz.	Improved impedance matching at lower frequency but introduced sharp band notches at 4 GHz and between 6 and 7 GHz.
T-shaped slits	To eliminate band notches by introducing slits.	Improved *BW* to 5.6 GHz and introduced additional 560 MHz of *BW* between 3 and 4 GHz	Effectively removed band notches with better impedance matching above 5 GHz.

In order to verify these results, a transient simulation was performed with a high-mesh setting (with a minimum of 20 lines per wavelength), resulting in approximately 550,000 mesh cells. The result is presented in Fig. 22(b). It is observed that the high-mesh S_{11} response shifts towards higher frequencies by almost 200 MHz, while S_{11} degradations are evident at 4.2, 5.2 and 6.2 GHz. To improve this, two additional topology modifications are implemented. Firstly a tapering of the feed line to the upper radiator (marked as E), and secondly, using different upper radiator widths (marked as $W1$ and $W2$). The optimal values are found to be $E = 2$ mm, $W1 = 13$ mm and $W2 = 16$ mm. The final topology with all additional modifications, referred to as ATA-FGP (all-textile antenna with full ground plane) is shown in Fig. 23(a). It features a 6.8 GHz bandwidth from 3.4 to 10.2 GHz as shown in Fig. 23(b). In summary, Table 4 provides an overview of all the techniques used and their contribution in achieving the UWB band, while keeping the full ground plane intact.

4. EXPERIMENTAL VERIFICATION

Final dimensions and fabricated prototype of the ATA-FGP are shown in Fig. 24 and Table 5. In the final topology, four top radiators can be seen. The probe feeds a small microstrip line which in turn feeds the three primary radiators A, B, and C. The ATA-FGP is then

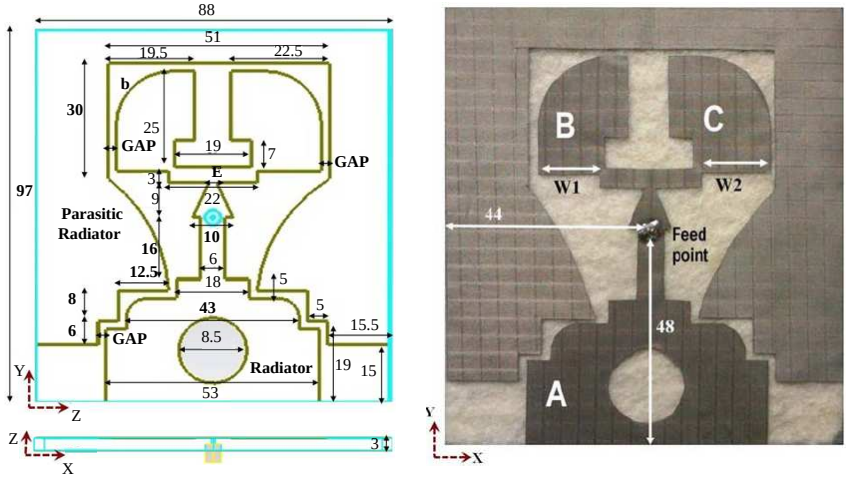

Figure 24. ATA-FGP (dimensions in mm) and its fabricated prototype.

evaluated for its S_{11}, radiation pattern (RP) and realized gain (G) in free space (FS). Simulation indicated antenna operation from 3.4 to 10.2 GHz, whereas measurements confirmed its functionality between 3.6 and 10.3 GHz with a bandwidth (BW) of 6.7 GHz. There is thus a slight shift by ca. 200 MHz to higher frequencies and a ca. 100 MHz BW reduction. Both S_{11} evaluations are shown in Fig. 25. Radiation patterns are evaluated in the x-z and y-z planes, as noted in Fig. 24, at three frequencies, i.e., 4 GHz, 7 GHz and 10 GHz. The simulated and measured RP shown in Fig. 26 show a good agreement. At 4 GHz it is observed that the ATA-FGP exhibits a reasonably directive radiation pattern towards boresight in the x-z plane. Meanwhile, an omni-directional behavior is generated in the y-z plane, which is an extremely suitable antenna characteristic for WBAN applications [3]. Similar patterns are seen in both planes at 7 and 10 GHz, with more obvious ripples at the higher 10 GHz frequency. To highlight the effect of the full ground plane, a comparison of simulated and measured front to back ratio (FBR) and realized gain at 4, 7, and 10 GHz is given in Table 6. The agreement between simulations and measurements is satisfactory.

In order to show the positive effect of the unidirectionality of this microstrip topology measurements on body (OB) were also performed. A simplified two-third muscle equivalent homogenous body model [3], sized at $131 \times 121 \times 44\,\text{mm}^3$ was used. Its relative permittivity is

Table 5. ATA-FGP parameters.

Parameter	Dim. (mm)	Remarks
Gap	2	Minimum gap between main radiator and parasitic radiator
E ($2e$)	$e = 1$	Length of horizontal feed line between $W1$ and $W2$
b (blend)	14	Blending radius of patches B and C

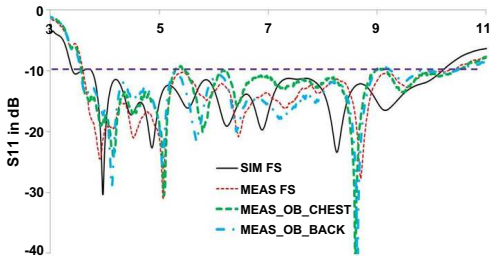

Figure 25. Simulated and measured S_{11} result in FS and OB.

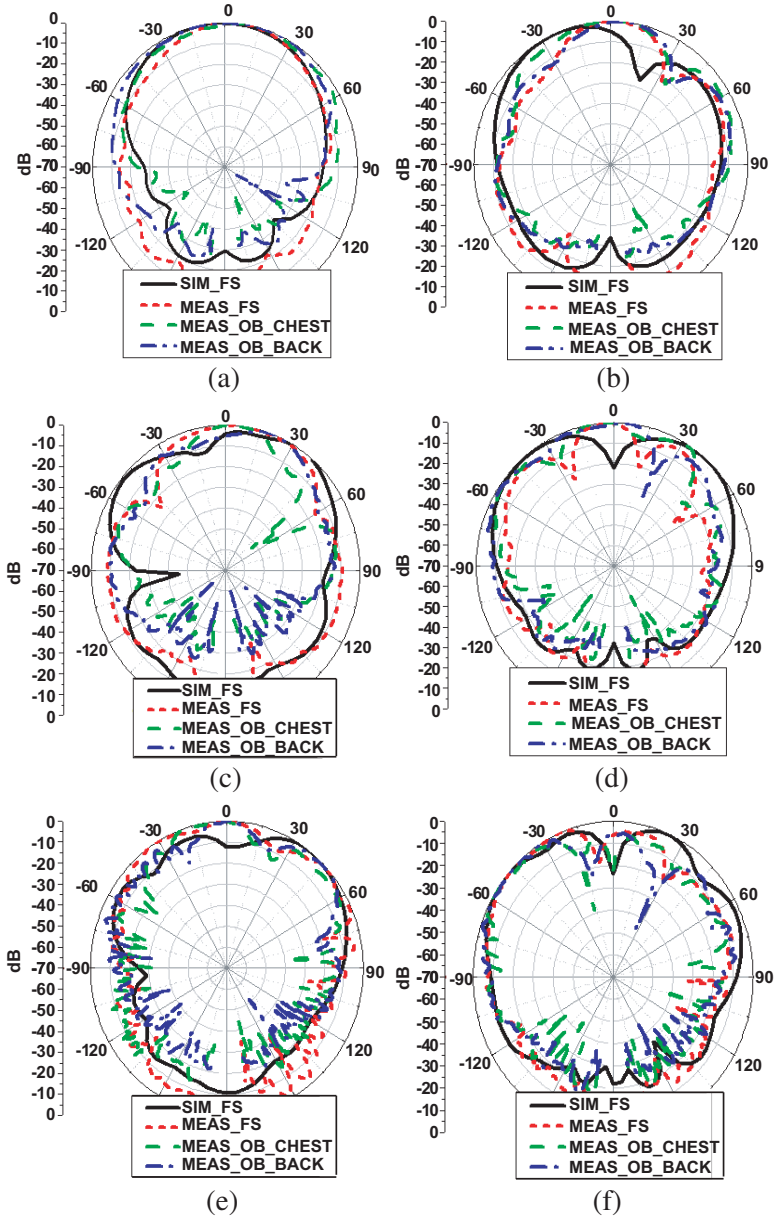

Figure 26. Simulated and measured radiation patterns in FS and OB for (a) x-z plane at 4 GHz, (b) y-z plane at 4 GHz, (c) x-z plane at 7 GHz, (d) y-z plane at 7 GHz, (e) x-z plane at 10 GHz, and y-z plane at 10 GHz.

Table 6. Front-to-back ratio (FBR) and realized gain (G) comparison.

Freq. (GHz)	Plane	Front-to-back ratio (FBR) (dB)		Realized gain (G) (dB)	
		Sim.	Meas.	Sim.	Meas.
4	x-z	25.0	12.2	6.13	8.07
	y-z	25.0	14.0		
7	x-z	18.0	20.0	5.31	4.72
	y-z	18.0	18.0		
10	x-z	9.0	9.5	6.98	5.67
	y-z	10.0	10.0		

Table 7. Comparison with other UWB antennas from literature.

Ref No.	Antenna structure	Material	*BW* (GHz)	Feed type	Ground plane (GP)	Effects of the presence of human body
This work	Microstrip antenna with co-axial feed	Shieldlt Super, Felt	6.7	Co-axial	Full GP	In proximity of human body, total BW is preserved
[15]	Circular UWB wearable antenna with slits	Jeans copper tape	9	Microstrip line	Partial GP	
[15]	Circular UWB wearable antenna with slits and center hole	Jeans copper tape	11.5	Microstrip line	Partial GP	
[16]	CPW Fed UWB disc monopole	Acrylic fabric, Nora	~ 6.5	CPW	-	
[16]	Microstrip Fed UWB annular slot antenna	Acrylic fabric, Nora	~ 7.5	Microstrip line	Slotted GP	Significant drop in S_{21} (up to 9 dB) between 3 and 8 GHz compared with FS
[2]	UWB button antenna-planar monopole	Metallic disc, PTFE, denim material	7.6	Microstrip line	Partial - square GP	
[29]	Circular slot CPW antenna	Shieldlt Super, Felt	7.2	CPW	-	S_{11} totally different in FS and OB, BW differs by ca. 460 MHz
[29]	Rectangular slot CPW antenna	Shieldlt Super, Felt	5.8	CPW	-	S_{11} totally different in FS and OB, BW differs by ca. 120 MHz

50.8 and its conductivity is 3 S/m. OB simulations were performed with the proposed ATA-FGP centered above this tissue model with an air gap of 10 mm. This air gap emulates a realistic approximation of the actual placement of the ATA-FGP on a human body with clothing [6, 17]. Experimental OB evaluations were performed with the

ATA-FGP placed on two locations: on the chest and back of a male human volunteer. This volunteer (height 1.58 m and weight 55 kg) wore everyday clothing with ca. 5 mm in thickness to emulate real situations. The on body S_{11} are shown also in Fig. 25. Despite the degradation of S_{11} by several decibels when evaluated OB, the available BW is preserved. This highlights the robustness of the designed ATA-FGP on body, mainly achieved due to the presence of a full ground plane.

In general, radiation patterns in FS and OB are similar. An obvious reduction in back radiation is observed OB. It is thus seen that with the presence of the full ground plane, the radiation pattern is also preserved when placed OB. Note that due to the presence of the human body, ripples are seen in both the xz and yz plane when φ is beyond $\pm 60^\circ$. Among others, this is due to the ATA-FGP's position, which is no longer in the transmitter's line-of-sight (LOS), such that most of the received power is gathered either through reflection or diffraction. This causes the ripples in the measured OB radiation patterns [13]. Moreover, the human body itself acts as a reflector at higher frequencies distorting the radiation pattern [3]. This effect is observed especially at 10 GHz with more visible ripples. A shadowing effect by the human body is also observed with sharp nulls at 7 GHz (xz plane, $\varphi = 60^\circ$) and 10 GHz (yz plane, $\varphi = 30^\circ$) [28].

Table 7 presents a comparison of the proposed microstrip antenna against previous UWB antennas. Note that most of them target body-worn applications. This is the reason why they are fabricated from flexible conductors or textile materials. These UWB antennas achieve ultra wide band behavior by either using CPW-fed topologies [16, 29] or microstrip-fed topologies with slotted or partial ground planes [2, 15, 16]. The presented coaxially-fed UWB microstrip antenna topology (ATA-FGP) is the only one successfully producing the desired UWB behaviour while keeping the full ground plane intact. In column 7 of this table, the effect of the presence of the body on the antenna is summarized in the cases where this information could be extracted from the papers. It is clearly seen that for the other antennas, the presence of the body has a drastic effect.

5. CONCLUSION

A design roadmap that creatively combines a range of broadbanding techniques with the specific goal to produce a very wide bandwidth (up to UWB) using microstrip technology has been presented. In many novel applications, especially for WBAN, the presence of the full microstrip ground plane offers huge advantages, such as unidirectionality and immunity to body detuning. The description started from a very simple basic structure that has been gradually

improved and has become more and more complex with each broadbanding step. The effect of each step has been clearly demonstrated by consistently comparing the antenna "before and after", both concerning matching and radiation characteristics. The resulting demonstrator antenna successfully reaches UWB behavior, both in simulations and measurements. However, this demonstrator is not the only specific topology possible. The same design roadmap can easily lead to other topologies, depending on the choices made at decision points in the design procedure.

ACKNOWLEDGMENT

This work is financially-supported in part by the EU-EXPERTS Program, the IEEE Microwave Theory and Techniques Society (MTT-S) Graduate Fellowship in Medical Applications, the Malaysian Ministry of Education (Higher Education Sector) and the Hercules Foundation. The authors acknowledge the technical contributions of Dr. Vladimir Volskiy, Dr. Zhongkun Ma and Dr. Hadi Aliakbarian from ESAT-TELEMIC, KU Leuven.

REFERENCES

1. "FCC report and order for Part 15: Acceptance of ultra wideband (UWB) systems from 3.1–10.6 GHz," Federal Communications Commission (FCC), 2002.
2. Sanz-Izquierdo, B., J. C. Batchelor, and M. I. Sobhy, "Compact UWB wearable antenna," *Loughborough Antennas and Propagation Conference*, 121–124, Apr. 2–3, 2007.
3. Chahat, N., M. Zhadobov, R. Sauleau, and K. Ito, "A compact UWB antenna for on-body applications," *IEEE Transactions on Antennas and Propagation*, Vol. 59, No. 4, 1123–1131, Apr. 2011.
4. Baskaran, K., C. P. Lee, and C. K. Chakrabarty, "A compact microstrip antenna for ultra wideband applications," *European Journal of Scientific Research*, Vol. 67, No. 1, 45–51, 2011.
5. Alomainy, A., Y. Hao, C. G. Parini, and P. S. Hall, "Comparison between two different antennas for UWB on-body propagation measurements," *IEEE Antennas and Wireless Propagation Letters*, Vol. 4, 31–34, 2005.
6. Soh, P. J., S. J. Boyes, G. A. E. Vandenbosch, Y. Huang, and S. L. Ooi, "On-body characterization of dual-band all-textile PIFAs," *Progress In Electromagnetic Research*, Vol. 129, 517–539, 2012.

7. Soh, P. J., G. A. E. Vandenbosch, S. L. Ooi, and M. R. N. Husna, "Wearable dual-band Sierpinski fractal PIFA using conductive fabric," *Electronics Letters*, Vol. 47, No. 6, 365–367, Mar. 2011.
8. Boyes, S. J., P. J. Soh, Y. Huang, G. A. E. Vandenbosch, and N. Khiabani, "On-body performance of dual-band textile antennas," *IET Microwaves, Antennas and Propagation*, Vol. 6, No. 15, 1696–1703, Dec. 2012.
9. Lilja, J., P. Salonen, T. Kaija, and P. D. Maagt, "Design and manufacturing of robust textile antennas for harsh environments," *IEEE Transactions on Antennas and Propagation*, Vol. 60, No. 9, 4130–4140, Sep. 2012.
10. Yoon, H. K., W. S. Kang, Y. J. Yoon, and C.-H. Lee, "A CPW-fed flexible monopole antenna for UWB systems," *IEEE Antennas and Propagation Society International Symposium*, 701–704, Jun. 9–15, 2007.
11. Gupta, S., M. Ramesh, and A. T. Kalghatgi, "Design of optimized CPW fed monopole antenna for UWB applications," *Asia-Pacific Microwave Conference*, 4–7, Dec. 2005.
12. Tran, D., F. M. Tanyer-Tigrek, A. Vorobyov, I. E. Lager, and L. P. Ligthart, "A novel CPW-fed optimized UWB printed antenna," *European Conference on Wireless Technologies*, 40–43, Oct. 8–10, 2007.
13. John, M., M. J. Ammann, and P. McEvoy, "UWB vivaldi antenna based on a spline geometry with frequency band-notch," *IEEE Antennas and Propagation Society International Symposium*, 1–4, Jul. 5–11, 2008.
14. Bai, J., S. Shi, and D. W. Prather, "Modified compact antipodal vivaldi antenna for 4–50-GHz UWB application," *IEEE Transactions on Microwave Theory and Techniques*, Vol. 59, No. 4, 1051–1057, Apr. 2011.
15. Osman, M. A. R., M. K. Abd Rahim, M. Azfar Abdullah, N. A. Samsuri, F. Zubir, and K. Kamardin, "Design, implementation and performance of ultra-wideband textile antenna," *Progress In Electromagnetics Research B*, Vol. 27, 307–325, 2011.
16. Klemm, M. and G. Troester, "Textile UWB antennas for wireless body area networks," *IEEE Transactions on Antennas and Propagation*, Vol. 54, No. 11, 3192–3197, Nov. 2006.
17. Soh, P. J., G. A. E. Vandenbosch, S. L. Ooi, and N. H. M. Rais, "Design of a broadband all-textile slotted PIFA," *IEEE Transactions on Antennas and Propagation*, Vol. 60, No. 1, 379–384, Jan. 2012.

18. Balanis, C. A., *Antenna Theory Analysis and Design*, 3rd Edition, Wiley and Sons, New York, 2005.
19. "CST microwave studio," Darmstadt, Germany: CST-Computer Simulation Technology AG, 2012.
20. Goudah, M. and M. Y. M. Yousef, "Bandwidth enhancement techniques comparison for ultra wideband microstrip antennas for wireless application," *Journal of Theoretical and Applied Information Technology*, Vol. 35, No. 2, 184–193, Jan. 2012.
21. Koohestani, M. and M. Golpour, "U-shaped microstrip patch antenna with novel parasitic tuning stubs for ultra wideband applications," *IET Microwaves, Antennas and Propagation*, Vol. 4, No. 7, 938–946, Jul. 2010.
22. Abdelaziz, A. A., "Bandwidth enhancement of microstrip antenna," *Progress In Electromagnetics Research*, Vol. 63, 311–317, 2006.
23. Fei, P., Y.-C. Jiao, and W. Hu, "A compact CPW-fed finger-shaped antenna for UWB application," *International Symposium on Antennas Propagation and EM Theory*, 79–82, Nov. 29–Dec. 2, 2010.
24. Chen, H.-D., "A dual-frequency rectangular microstrip antenna with a circular slot," *Microwave and Optical Technology Letters*, Vol. 18, No. 2, 130–132, Jun. 1998.
25. Liu, W.-C., C.-M. Wu, and Y.-J. Tseng, "Parasitically loaded CPW-fed monopole antenna for broadband operation," *IEEE Transactions on Antennas and Propagation*, Vol. 59, No. 6, 2415–2419, Jun. 2011.
26. Rahayu, Y., R. Ngah, and T. A. Rahman, "A small novel ultra wideband antenna with slotted ground plane," *International Conference on Computer and Communication Engineering*, 677–682, May 13–15, 2008.
27. Patil, V. P., "Enhancement of bandwidth of rectangular patch antenna using two square slots techniques," *International Journal of Engineering Sciences and Emerging Technologies*, Vol. 3, No. 2, 1–12, Oct. 2012.
28. Ruckveratham, B., S. Teawehim, P. Chiochan, and S. Promwong, "Evaluation of ultra wideband body area network," *Biomedical Engineering International Conference*, 311–315, Jan. 29–31, 2011.
29. Soh, P. J., G. A. E. Vandenbosch, and J. Higuera-Oro, "Design and evaluation of flexible CPW-fed ultra wideband (UWB) textile antennas," *IEEE International RF and Microwave Conference (RFM)*, 133–136, Dec. 12–14, 2011.